

# Friction coefficient behaviour between rubber wheel and hydraulic concrete under different contact conditions

N. Santander Reyes and E. Gallardo Hernández

*Instituto Politécnico Nacional, SEPI-ESIME, Zacatenco,  
Grupo de Tribología. Col. Lindavista, 07738, Ciudad de México, México.*

E. E. Vera Cárdenas

*Tecnológico Nacional de México/Instituto Tecnológico de Pachuca,  
Col. Venta Prieta, Pachuca, 42083, Hidalgo, México.  
e-mail: edgar.vc@pachuca.tecnm.mx*

Received 15 May 2024; accepted 13 December 2024

Currently, some countries are implementing the Bus Rapid Transit (BRT) system which combines the efficiency and quality of the Metro system and offers flexibility and low cost of infrastructure. To ensure the safety of users, the study of friction in pneumatic wheels in different environmental contaminants must be tested for these vehicles, since they carry out some fundamental functions like driving transmission, traction and braking. In this study, the behaviour of the coefficient of friction between SBR rubber and hydraulic concrete MR 48 was analysed in different contact conditions. Properties of SBR rubber were obtained with a universal testing machine and a durometer shore A, while the properties of concrete MR 48 were obtained with a compression testing machine. The friction experiments were performed by using the British pendulum method. Micrographs of the rubber surface were obtained by scanning electron microscope. The results showed that high values of coefficient of friction are obtained in dry condition and even higher at tests with temperature of 35°C. Contrary, the lowest coefficients of friction were seen in wet condition and with contaminants. However, for the wet condition the coefficient of friction can recover after applying silica sand.

**Keywords:** British pendulum; friction; hydraulic concrete; rubber wheel; contaminant.

DOI: <https://doi.org/10.31349/RevMexFis.71.031005>

## 1. Introduction

Throughout the world, the extensive use of the automobile is not the only factor that contributes to the emission of greenhouse gases, it also causes air pollution in cities. A transport system that has given good results in countries like Mexico, Colombia, Brazil, Guatemala, Ecuador, Chile, Peru, Argentina between others is the Bus Rapid Transit (BRT) system [1]. BTR systems are not only much cheaper and faster to build than Metro, they also provide similar reductions in travel times. This collective transport uses an exclusive lane made of hydraulic concrete [2]. The use of hydraulic concrete on public transport roads for articulated vehicles in addition to other type of road sections is increasing due to its high resistance to deformation and lower maintenance cost compared to asphalt roads [3-5]. Concrete roads must provide the appropriate frictional forces with the tires to carry out some emergency functions like taking curves, braking, traction and driving [6]. According to some authors, the contact between the pneumatic tire and the pavement, mainly results in two friction mechanisms, which are adhesion and hysteresis. Adhesion is a phenomenon whereby the atoms of two bodies in contact, rigid or not, develop small electromagnetic forces of mutual traction. Hysteresis is the resulting frictional force caused by the loss of energy due to the deformation in the tire of the vehicle. Due to the operation of a vehicle, the tire is compressed with a uniform distribution of stress, lead-

ing to storage of deformation energy in the rubber structure. On the other hand, when the tire is unloaded, part of the energy is recovered, while the rest is dissipated as heat (hysteresis) [7-14]. According to some transport regulations, an optimal coefficient of friction between the tire and pavement is considered in the range from 0.61 to 0.8, good from 0.81 to 0.9, regular from 0.51 to 0.6, and bad when is below 0.5 or greater than 0.91 [15]. Some works have been done using the British pendulum, proposing an experimental methodology to evaluate the friction on steel tracks for the rubber tired Metro evaluating different surfaces textures [16]. Another work performed with the same equipment was to evaluate the coefficient of friction in pavement covered with ice, as well as the use of sand dispersed on the ice surface as a friction improver [17]. B. N. J. Persson *et al.*, studied the frictional behaviour of rubber on wet condition, in which it was demonstrated that the type of contact between rubber and a solid surface cannot be hydrodynamic. Water smooth the surface, which reduces the main friction due to the viscoelastic properties of rubber induced by surface roughness [18]. T. Vieira *et al.*, assessed wear rates and friction mechanisms of rubber. The rubber specimens used for the tests were obtained from a common commercial tire, a green tire and a racing tire by using the British pendulum [19]. S. Changarnier *et al.*, conducted an investigation on how dust accumulation affects the tire-road interaction measuring the coefficient of friction with

a pendulum device [20]. Y. Hichiri *et al.*, presented a model that expresses the surface cover by fine particles. The research is based on the identification of particle flows between the pneumatic tire and the road. The images revealed an expulsion flow and a recirculation flow composed of particles lifted by the slider [21]. J. Karger-Kocsis *et al.*, conducted a study of friction and wear in dry condition by sliding of an EPDM rubber against steel. The rubber used had different concentrations of carbon black and different configurations of the test machine were used such as pin on plate and ring on plate. It was found that with the increase in carbon black content the specific wear rate tended to reduce as did the coefficient of friction [22]. D. Xu in collaboration with J. Karger-Kocsis, determined the friction and wear by rolling of the rubbers EPDM and SBR with different contents of carbon black against steel. It was concluded that the addition of carbon black increases the hardness and the coefficient of friction (the latter marginally) and decreases the specific wear rate for both EPDM and SBR [23]. Y. Fukahori *et al.*, carried out a study on the characteristic pattern of abrasive wear on SBR rubber. For these experiments an abrasion machine was used. It was possible to observe the characteristic ridges of abrasion wear and the angle at which they are formed at  $30^\circ$  and  $50^\circ$  [24]. Fangman Xu *et al.*, studied the impact of surface roughness of rubber on slip friction using a pin on disk configuration. Friction coefficient was obtained utilizing textured samples and flat samples (not textured). In dry conditions, textured specimens, showed low coefficients of friction. Under lubricated condition and using low speeds, the friction coefficients were higher, but those were lower in a higher speed region, concluding that the lubrication conditions should be applied on the surface of the rubber [25]. C. Khelifi *et al.*, investigated the change of the resistance to sliding of various materials of subway tracks. Three materials were studied of which two were mixtures of concrete and the other one was steel. The experimental results indicate that concrete improved slip resistance compare to steel, while initial slip resistance at the start depends on the treatment ap-

plied on the surface texture [26]. Dharamveer Singh *et al.*, analysed a mathematical model to evaluate the coefficient of friction between the pavement and the tire in wet conditions. The study was conducted on five different types of rubber samples. The coefficient of friction was measured using a British pendulum equipment in wet conditions. The theoretical friction coefficient was calculated by entering experimental data in the mathematical model. The results showed that wet adhesive friction was the main contributor to the theoretical friction coefficient, while dry adhesive friction was the lowest [27]. The purpose of this work is the determination of the coefficient of friction between the pneumatic wheel and the lane surface of the BRT system, simulating this contact with a pair of materials of a styrene butadiene rubber (SBR) against an MR 48 hydraulic concrete, which is evaluated in different environmental conditions by using the British pendulum device in laboratory. The environmental contaminants conditions selected are those that the BRT system of Mexico City is exposed.

## 2. Experimental procedure

### 2.1. Test materials

The behaviour of coefficient of friction between SBR (slider) and hydraulic MR 48 concrete (specimen) is studied using a British pendulum method. Hydraulic MR 48 concrete is the type of concrete that is being used in different types of roads and highways due to its high resistance to deformation and lower maintenance cost than asphalt roads [3-5]. To validate the specimens of MR 48 concrete, compression tests were performed according to the ASTM C39 [28] (Fig. 1), using a compression testing machine Soiltest model CT-750. The specimens were manufactured based on the ASTM C31 [29]. In order to have a uniform loading and in accordance with ASTM C1231 [30], neoprene pads are used at both ends of the concrete specimen to ensure uniform loading.



FIGURE 1. Compression test. a) Cylindrical concrete specimen. b) Tested specimen.

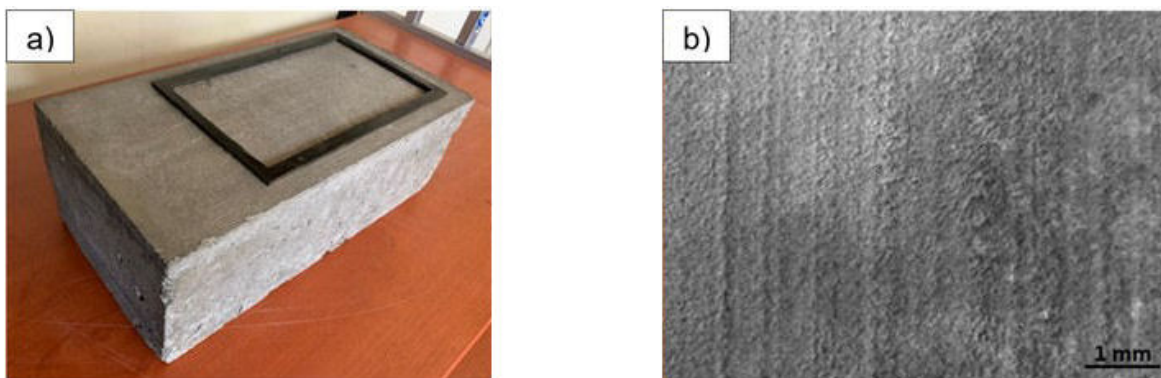


FIGURE 2. a) Concrete specimen, b) Surface of the concrete.

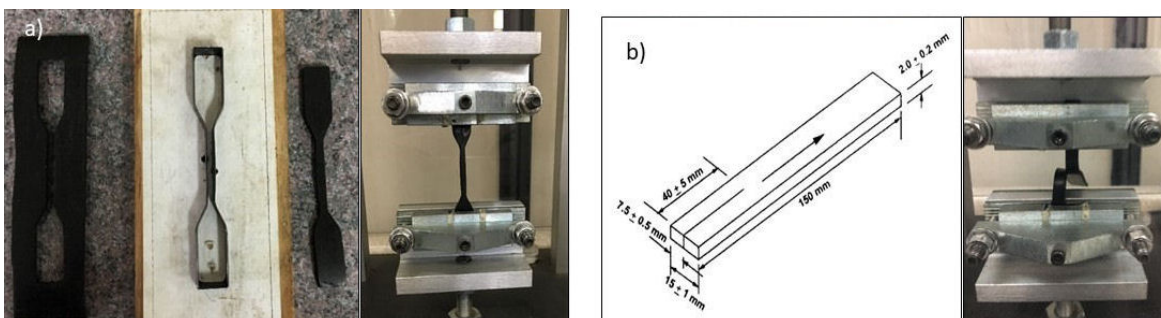


FIGURE 3. SBR mechanical tests. a) Tensile test. b) Shear strength test.

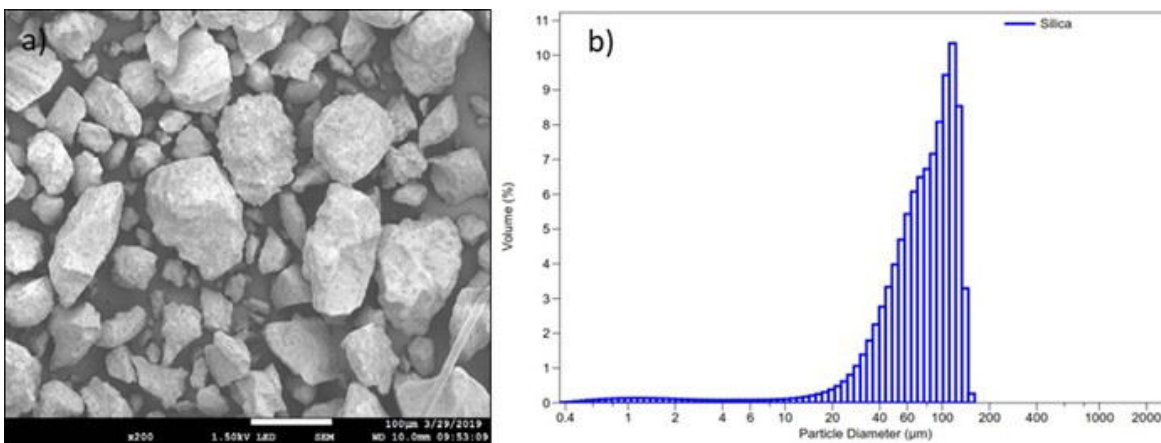


FIGURE 4. a) Morphology of particles. b) Particle size distribution.

The dimensions of concrete block MR 48 for friction tests with British pendulum are  $0.3 \times 0.15 \times 0.1$  m. Figure 2a) shows the block of concrete that works as specimen and in the Fig. 2b) the texture of surface can be seen.

The hardness Vickers and elastic modulus of MR 48 concrete were determined with a Berkovich indenter method. The roughness of the concrete surface in the parameters  $R_a$ ,  $R_q$ ,  $R_z$ ,  $R_{da}$ , and  $R_{dq}$  were determined using an optical profilometer BRUKER model Contour GT with a 5x objective lens. In the case of the SBR material, this was obtained from a commercial tire. Shore A hardness was measured with a DLXD SHORE durometer according to ASTM D2240 [31].

The tensile strength [Fig. 3a)] and shear strength [Fig. 3b)] of SBR were obtained with an universal testing machine Com-Ten with a separation rate of 85 mm/min consistently, according to ASTM D412 [32] and ASTM D624 [33], respectively. In the case of tensile testing, due to the flow grain anisotropy or directionality introduced during SBR processing and preparation, there may be an influence on the tensile properties, so the specimens are cut so that the longitudinal direction of the sample is parallel to the grain direction. The roughness of SBR slider specimen was determined using a Mitutoyo profilometer model SJ-410.

TABLE I. Test contact conditions.

Test condition	Contact length of 0.126 m	0.003 l of water	0.06 l of water	Heat contact surface	1 g of silica sand
Dry condition (T1)	✓				
Wet condition by spraying (T2)	✓	✓			
Wet flooded condition (T3)	✓		✓		
Temperature condition at 35°C (T4)	✓			✓	
Contaminant condition (T5)	✓				✓
Wet condition by spraying with contaminants (T6)	✓	✓			✓
Wet flooded condition with contaminants (T7)	✓		✓		✓

For the friction tests, in contaminant condition, silica sand was used due to the similarity with the particles accumulated on roads. Figure 4a) shows the morphology of the particles of silica sand using a SEM equipment model JEOL JSM-6610LV. Figure 4b) shows the particle size distribution of silica sand carried out with a diffraction laser equipment BECKMAN COULTER model LS 230, obtaining an average particle size of 80.7  $\mu\text{m}$ , and with a largest particle size of 121.8  $\mu\text{m}$ .

## 2.2. Friction tests equipment

The equipment used was the British pendulum, designed to simulate a sliding contact condition against a solid rigid surface under BS 7976-1 standard used especially for road [34]. An elastomer specimen is mounted at the end of the tubular arm which works with sliding speeds of 2 to 5 m/s, with a preload of 22 N, the sliding surface distance must be 0.126 m  $\pm$  0.001. The friction between the slider and the surface produces a loss of energy which is measured in SRV (Slip Resistance Value) by means of a pointer on the scale when the arm swings upwards (Fig. 5). The bounce height

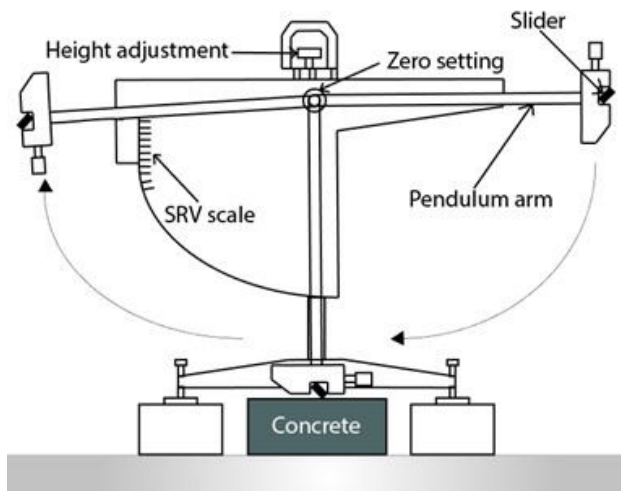


FIGURE 5. Schematic diagram of the British pendulum.

is equal to the slip resistance value that is measured on the pendulum scale. These values can be found almost roughly equal by multiplying  $\mu \times 100$ , however, due to the compression of the spring arrangement on the elastomer slider, there is a significant deviation [35], Eqs. (1) and (2) were used to determine the coefficient of friction.

$$\mu = \frac{3 * SRV}{110 - SRV}. \quad (1)$$

Factorizing Eq. (1)

$$\mu = \left( \frac{110}{SRV} - \frac{1}{3} \right)^{-1}. \quad (2)$$

## 2.3. Friction tests procedure

Six friction tests were performed in each test condition (Table I) according to ASTM E303 [36], verifying the correct calibration of the pendulum equipment and the contact length, the rubber sliders must also be conditioned prior to test with using sandpaper according to the test method (Fig. 6). In order to validate the tests results according to ASTM E303, Eq. (3) is used to determine the error [36].

$$E = (t\sigma n)^{-1/2}, \quad (3)$$

where  $E$  is the test error,  $t$  the normal curve from 1.96 or rounded to 2,  $\sigma$  is the standard deviation of the individual test results (SRV) and  $n$  the number of tests. In order to validate the tests, error must be minor than 1 SRV.

For temperature condition tests (T4) an infrared incandescent lamp was used to heat up uniformly the hydraulic concrete test surface at 35°C  $\pm$  2, the temperature was measured with a pyrometer. For contaminated condition tests (T5, T6 and T7) silica sand was used due to the similarity with the particles accumulated on roads during dry weather period having a size up to 125  $\mu\text{m}$  with a concentration from 10 g/m<sup>2</sup> to 55 g/m<sup>2</sup> [9,20]. Finally, some tests were carried out in wet condition (T2, T3, T6 and T7) to simulate light rain and when it rains heavily. It is important to analyse the wet condition due to the increase in accidents when it rains, additionally the wet tests were carried out with and without

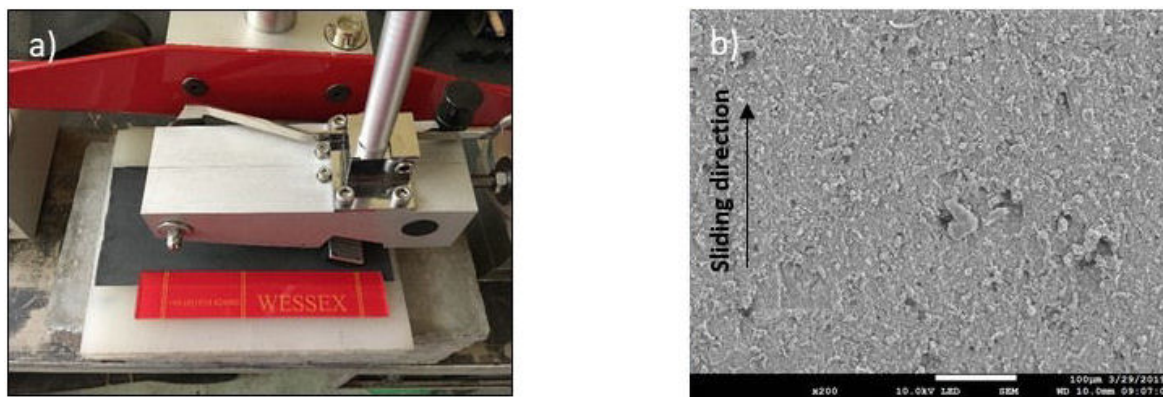


FIGURE 6. a) SBR slider preparation with silicon carbide sandpaper. b) Micrograph of the slider conditioned with sandpaper.

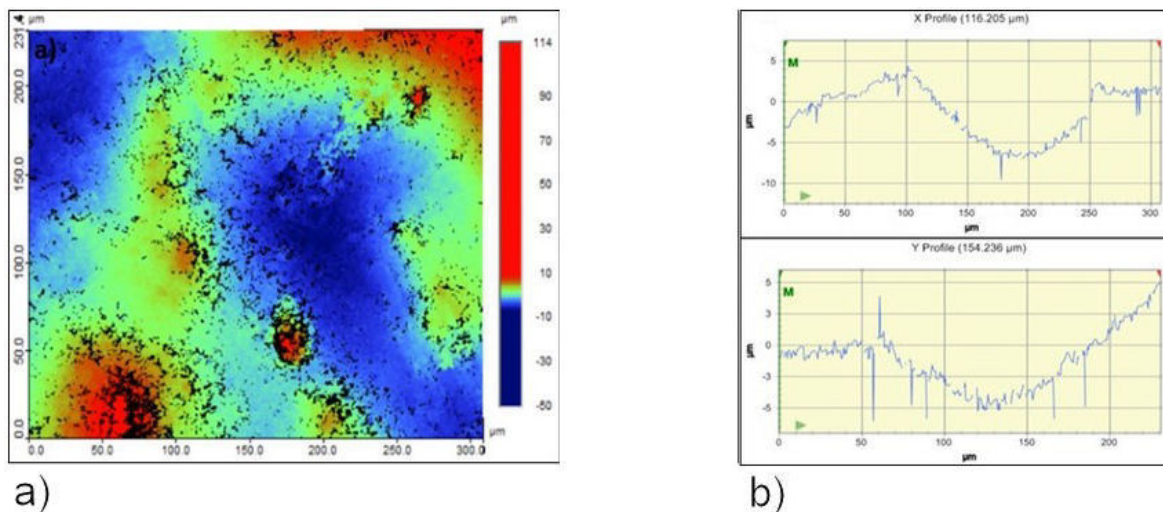


FIGURE 7. a) Mapping of the roughness, b) Roughness profile.

sand. For all the tests, the rubber slider was at room temperature ( $25^{\circ}\text{C} \pm 2$ ).

### 3. Results and discussion

#### 3.1. Roughness of MR 48 hydraulic concrete

The values of roughness parameters  $R_a$  ( $5.22 \mu\text{m}$ ),  $R_q$  ( $7.1 \mu\text{m}$ ),  $R_z$  ( $31.3 \mu\text{m}$ ) and slope parameters  $R_{da}$  ( $4.26^{\circ}$ ),  $R_{dq}$  ( $8.77^{\circ}$ ) were obtained. The values of  $R_a$ ,  $R_q$  and  $R_z$  indicate a rough surface of the block specimen as prepared according to ASTM C31, influencing the values of the friction coefficients obtained. In the case of the slope parameters, that describe the characteristics of the slope of the roughness profile, the obtained values reflect a profile with steep slopes, producing fragile behaviour on the surface crests. Figure 7a) shows a surface mapping of the roughness of the MR 48 concrete block and Fig. 7b) shows the roughness profile with respect to the  $x$ -axis and the  $y$ -axis in 2D.

#### 3.2. Mechanical properties

The mechanical properties of SBR and concrete MR 48 are shown in Table II. The values were obtained experimentally

as described in Sec. 2.1 and are according to those obtained in other works [37,38]. The average roughness  $R_q$  of SBR corresponds to the surface finish of a new commercial tire used in this study. The values of roughness of both materials provide important information on the behaviour of the coefficient of friction obtained in the experimental tests.

#### 3.3. Coefficient of friction and schematic models of contact rubber-concrete

Table III shows the friction results, while in Fig. 8 can be observed the average coefficient of friction. In wet condition by spraying there was a loss of friction of 58.1% with respect to dry condition. For wet flooded condition, the loss was of 44.59%. For temperature condition there was an increase of 5.4%. In contaminant condition there was a loss of friction of 43.24%. For the last two conditions in wet condition by spraying and flooded with contaminants occurred a loss of friction of 48.65% and 40.54% respectively. The discussion about the friction results is better explained below with the interpretation of the different schematic models of contact rubber-concrete, shown in Fig. 9.

TABLE II. Mechanical properties of SBR rubber and concrete MR 48.

SBR				
Elastic modulus	Hardness (Shore A)	Tensile strength	Shear strength	Roughness Rq
0.021 GPa	65.5	0.989 MPa	3036 Pa	0.8 $\mu\text{m}$
Hydraulic concrete MR 48				
Elastic modulus	Hardness (Vickers)	Compressive strength	Roughness Rq	
29.702 GPa	78.228	23.52 MPa	7.1 $\mu\text{m}$	

TABLE III. Friction results and test error.

Test condition	Test number						Average	Standard deviation	Test error
	1	2	3	4	5	6			
T1	0.78	0.75	0.74	0.74	0.72	0.72	0.74	0.02	0.23
T2	0.33	0.32	0.3	0.31	0.3	0.3	0.31	0.01	0.25
T3	0.41	0.41	0.4	0.41	0.43	0.41	0.41	0.008	0.35
T4	0.8	0.8	0.8	0.78	0.78	0.76	0.79	0.02	0.26
T5	0.41	0.41	0.43	0.41	0.41	0.43	0.42	0.009	0.44
T6	0.37	0.38	0.38	0.38	0.37	0.37	0.38	0.006	0.41
T7	0.44	0.45	0.44	0.45	0.44	0.43	0.44	0.007	0.41

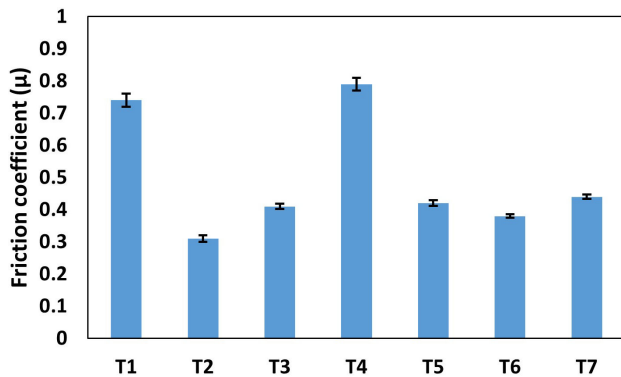


FIGURE 8. Friction coefficient average in different contact conditions.

In Fig. 9 the schematic models of the interaction between the elastomer slider against a concrete surface under each test condition are shown. It should be noted that for this work only the interaction of both materials in contact was considered without taking into account the grooves of the hydraulic concrete and neither the channels and the own design of the tire tread, this because the British pendulum is not designed to operate on a very rough surface with a macro texture. In dry condition tests (T1), the rubber deformed, this happened due to its low modulus of elasticity, filling up the ridges and valleys of the rough surface of the concrete; this deformation is expelled by heat in addition to the chemical and magnetic bonding of both materials [18]. During the experimental test in dry condition [Fig. 9a)] it was observed a decrease tendency of the friction coefficient between each test. Tests at wet condition with spray [Fig. 9b)] showed a

water film that fills the ridges and valleys of the rough surface on the concrete sample avoiding adhesion between the samples [18]. The minimum film thickness  $h_{\min}$  calculated is 0.10238  $\mu\text{m}$  and  $\Lambda$  ratio is 0.01279, so, the lubrication regime is boundary for the pendulum method [39]. In a flooded condition [Fig. 9c)], the slider must displace large amount of water. According to the Newtonian viscosity law, for a Newtonian fluid, the relationship between the effort and the cutting speed, which indicates that to displace that amount of water greater effort is needed, which is reflected in the loss of energy of the pendulum when impacts against the water film giving a friction reduction. The highest coefficient of friction was obtained at temperature condition at 35°C (T4) [Fig. 9d)] mainly due to the change on viscoelastic properties of the elastomer [18]. By increasing the temperature, relaxation times are reduced, because the molecules have greater mobility and require less time to readjust and the viscous forces are overcome by the kinetic energy, causing a decrease in the viscosity of the material, producing deformation and adhesion mechanisms on the surface that increase the friction. Sand particles decrease the coefficient of friction because some particles are deposited in the cavities of the peaks and valleys of the concrete surface reducing hysteresis friction and micro hysteresis [Fig. 9e)], while larger sand particles tend to roll, which facilitates the slider slip, however, the wear rate is greater because of the abrasive effect. The particle size has an effect on the friction coefficient would increase when particle size is larger [20]. Wet (atomized) condition with contaminant [Fig. 9f)] was similar to what was obtained in a contaminant condition, however, the deposited water film

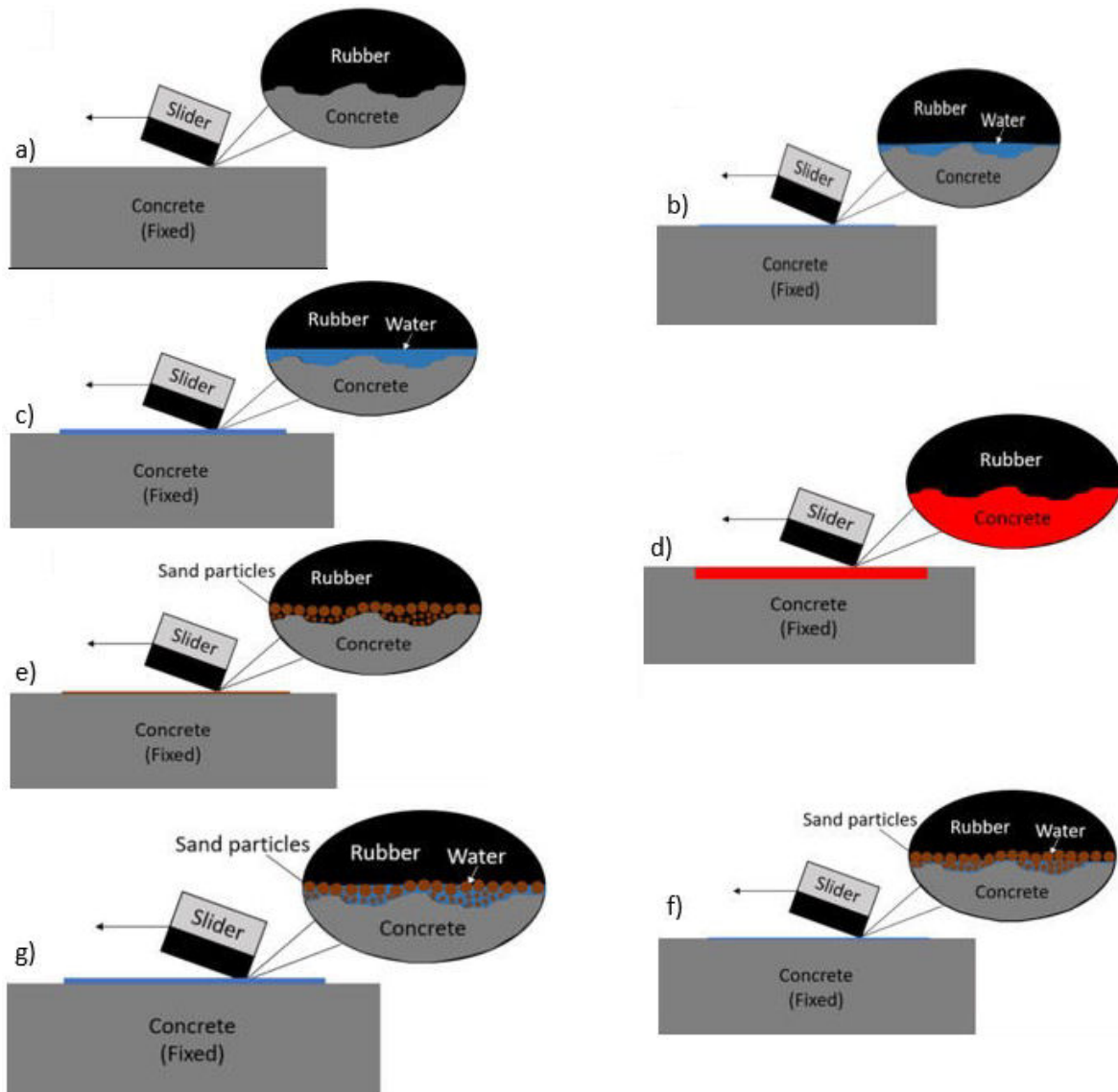


FIGURE 9. Schematic models of the series of test conditions: a) dry (T1), b) sprayed water (T2), c) flooded contact (T3), d) temperature condition (T4), e) dry and sand (T5), f) sand and sprayed water (T6), and g) sand and flooded contact (T7).

layer increases the coefficient of friction because the combination of sand particles with water forms a viscous layer [9,20]. In wet condition (flooded) with contaminant [Fig. 9g)], while particles of sand and water fill the valleys and ridges, the water layer increases the resistance to slipping, that is why is necessary a greater effort to break it.

### 3.4. SEM of SBR slider

In order to observe the surface of the elastomer in an electron microscope it was necessary to apply a coating of gold by physical vapour deposition (PVD). In Fig. 10e) can be observed the wear features of the slider after the series of tests according to the different conditions. Some abrasive mark along of the sliding direction, adhesive wear, tearing and scratches were observed.

In Fig. 10b) it can be observed certain abrasive patterns due to dry sliding contact, but unlike the initial condition with sandpaper, the size of ridges and valleys was reduced. In Fig. 10c) there are not abrasion patterns, instead there are areas with adhesive wear, in addition, it can be seen that the size of ridges and valleys was significantly reduced in comparison from which it is observed in dry condition and hence because a low coefficient of friction is obtained. Figure 10d) shows the elastomer slider in temperature condition, it can be seen areas with adhesive wear and tearing as well as areas with abrasion patterns and patterns similar to those obtained with the preparation with sandpaper. In Fig. 10e) the elastomer slider is shown in a contaminated condition, it can be observed areas with tearing, also the areas of ridges and valleys slightly smaller than the elastomer slider prepared with sandpaper.

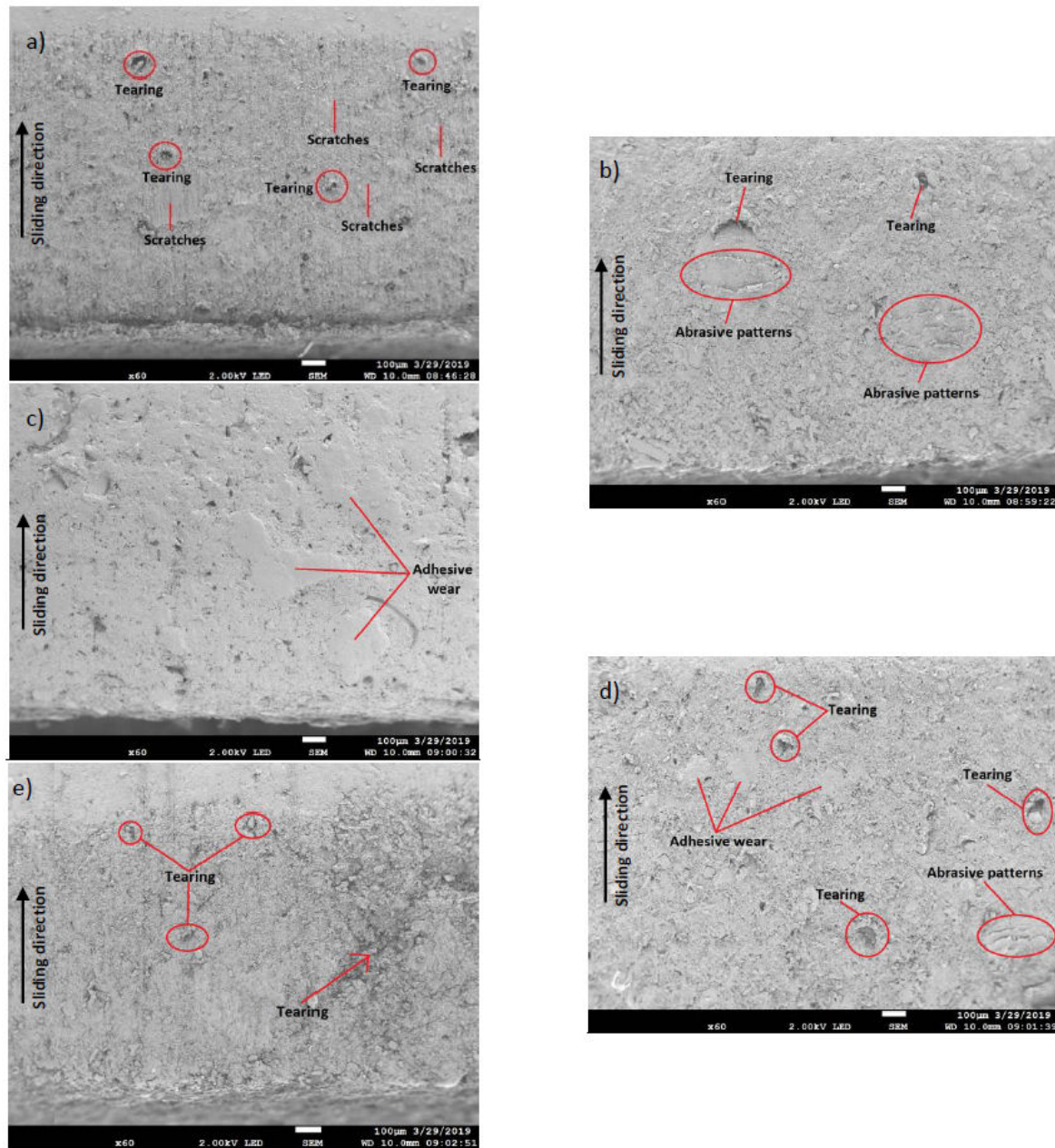


FIGURE 10. Slider surfaces; a) initial condition (with sandpaper), b) dry condition, c) wet condition by spraying, d) temperature condition, e) contaminant condition with sand.

#### 4. Conclusion

As it was expected, friction coefficient was affected showing high values in dry conditions, both at room temperature and at temperature of  $35^{\circ}$ . Low friction coefficients were obtained when separately water and sand was applied. Coefficient of friction was low when the combination of water and sand, flooded contact and sprayed water was separately added too. In the tests at temperature condition of  $35^{\circ}\text{C}$  the highest friction was presented, mainly due to the change on viscoelastic properties of the rubber. In the tests with contaminant, where silica sand particles were added, an increase in the friction was observed, both in dry and wet conditions.

The hydraulic concrete showed to have the best performance in adhesion with the SBR rubber when the temperature increases. This could have a good impact and demonstrates why this material is widely used in BRT systems, where different environmental conditions are presented, besides its low maintenance cost. It should be noted that the minimum friction value allowed on roads in Mexico is 0.5 this is in general regardless of whether the roads are made of asphalt or hydraulic concrete, however, in this work only the interaction of both materials in contact was evaluated without considering the grooves, that is why in wet condition it was got a low coefficient of friction. In future work, the texturing of concrete and rubber would be considered to evacuate water and

allow greater adhesion between concrete and rubber, in addition to mitigate the water layer between both surfaces and also avoiding the phenomenon of aquaplaning.

### Funding

This research received no specific grant from any funding agency in the public, commercial, or not-for-profit sectors.

### Declaration of conflicting interests

The Authors declare that there is no conflict of interest.

1. D. A. Rodriguez, E. Vergel, Bus rapid transit and urban development in latin America, *Land Lines* **25** (2013) 14.
2. J. P. Bocarejo, I. Portilla, M. A. Pérez, Impact of transmilenio on density, land use, and land value in Bogotá, *Research in Transportation Economics* **40** (2012) 78, <https://doi.org/10.1016/j.retrec.2012.06.030>.
3. I. Kamal, Y. Bas, Materials and technologies in road pavements - an overview, *Materials Today* **42** (2021) 2660, <https://doi.org/10.1016/j.matpr.2020.12.643>.
4. C. Teerawattanasuk and P. Voottipruex, Comparison between cement and fly ash geopolymer for stabilized marginal lateritic soil as road material, *International Journal of Pavement Engineering*, **20** (2019) 1264. <https://doi.org/10.1080/10298436.2017.1402593>.
5. N. A. Khalifa, A. Zulkiple and M. Ogab, The impact of different road damage factors on the pavement of local roads (JKR U2/U3) in Malaysia, *Int. J. Pavement Res. Technol.* **13** (2020) 240, <https://doi.org/10.1007/s42947-020-0190-1>.
6. Z. Rado and M. Kane, An initial attempt to develop an empirical relation between texture and pavement friction using the HHT approach, *Wear* **309** (2014) 233, <https://doi.org/10.1016/j.wear.2013.11.015>.
7. K. L. Smith, J. W. Hall, L. Titus-Glover, Guide for Pavement Friction. *Contract. Final Rep. NCHRP Proj. 01-43* (2009) 75,
8. N. K. Myshkin, M. I. Petrokovets, A. V. Kovalev, Tribology of polymers: Adhesion, friction, wear, and mass-transfer, *Tribol Int* **38** (2005) 910, <https://doi.org/10.1016/j.triboint.2005.07.016>.
9. Y. Hichri *et al.*, Friction on road surfaces contaminated by fine particles: Some new experimental evidences, *Proc Inst Mec. Eng Part J J Eng Tribol* **231** (2017) 1209, <https://doi.org/10.1177/1350650117704345>.
10. X. Xie *et al.*, Influence of temperature on polishing behaviour of asphalt road surfaces, *Wear* **402-403** (2018) 49, <https://doi.org/10.1016/j.wear.2018.02.002>.
11. G. Heinrich, Hysteresis Friction of sliding rubbers on rough and fractal surfaces. *Rubber Chem Technol* **70** (1997) 1, <https://doi.org/10.5254/1.3538415>.
12. C.L. Dong *et al.*, Tribological properties of aged nitrile butadiene rubber under dry sliding conditions, *Wear* **322-323** (2015) 226, <https://doi.org/10.1016/j.wear.2014.11.010>.
13. A. Le Gal *et al.*, Modelling of sliding friction for carbon black and silica filled elastomers on road tracks, *Wear* **264** (2008) 606, <https://doi.org/10.1016/j.wear.2007.05.002>.
14. G. Heinrich, M. Klüppel, Rubber friction, tread deformation and tire traction, *Wear* **265** (2008) 1052, <https://doi.org/10.1016/j.wear.2008.02.016>.
15. D. B. López Valdés, P. Garnica Anguas, Consideraciones para la aplicación del índice de fricción internacional en carreteras de México, Secretaría de Comunicaciones y Transportes, Instituto Mexicano del Transporte Publicación Técnica No. 170 (2002).
16. M. Moreno Ríos, Obtención de Coeficientes de Fricción con equipo Péndulo en Contactos Rueda-Riel de Sistemas Ferroviarios, Doctoral Thesis, Instituto Politecnico Nacional, Sección de Estudios de Posgrado e Investigación, Ciudad de México, México, (2015).
17. A. Hurtado Mayen, Estudio del coeficiente de fricción en asfalto con presencia de hielo y arena empleando el péndulo deslizante, Master Thesis, Instituto Politecnico Nacional, Sección de Estudios de Posgrado e Investigación, Ciudad de México, México, (2017).
18. B. N. J. Persson *et al.*, Rubber friction on wet and dry road surfaces: The sealing effect, *Phys. Rev. B* **71** (2005) 035428, <https://doi.org/10.1103/PhysRevB.71.035428>.
19. T. Vieira *et al.*, Evaluation of friction mechanisms and wear rates on rubber tire materials by low-cost laboratory tests, *Wear* **328-329** (2015) 556, <https://doi.org/10.1016/j.wear.2015.04.001>.
20. S. Changarnier *et al.*, Observations of dry particles behaviour at the tyre/road interface, *Tribol Int.* **128** (2018) 291, <https://doi.org/10.1016/j.triboint.2018.07.023>.
21. Y. Hichri, V. Cerezo, M. T. Do, Modeling of the surface coverage and application to the calculation of friction on surfaces contaminated by particles, *Wear* **426-427** (2019) 1082, <https://doi.org/10.1016/j.wear.2018.12.086>.
22. J. Karger-Kocsis *et al.*, Dry friction and sliding wear of EPDM rubbers against steel as a function of carbon black content, *Wear* **264** (2008) 359, <https://doi.org/10.1016/j.wear.2007.03.021>.
23. D. Xu, J. Karger-Kocsis, A. K. Schlarb. Rolling wear of EPDM and SBR rubbers as a function of carbon black contents: Correlation with micro hardness, *J. Mater. Sci.* **43** (2008) 4330, <https://doi.org/10.1007/s10853-008-2637-7>.

24. Y. Fukahori, H. Liang, J. J. C. Busfield, Criteria for crack initiation during rubber abrasion, *Wear* **265** (2008) 387, <https://doi.org/10.1016/j.wear.2007.11.008>.
25. F. Xu, K. Yoshimura, H. Mizuta, Experimental study on friction properties of rubber material: Influence of surface roughness on sliding friction, *Procedia Eng* **68** (2013) 19, <https://doi.org/10.1016/j.proeng.2013.12.141>.
26. C. Khelifi, M. Kane, M. A. Meyer. Evolution of skid resistance of different materials for Metro rolling tracks. 2016 International Conference on Sustainable Energy, Environment and Information Engineering (SEEIE 2016), Bangkok, Thailand, March (2016) 548-551.
27. D. Singh *et al.*, Evolution of coefficient of friction between tire and pavement under wet conditions using surface free energy technique, *Constr Build Mater* **204** (2019) 105, <https://doi.org/10.1016/j.conbuildmat.2019.01.122>.
28. ASTM C39 Test method for compressive strength of cylindrical concrete specimens. ASTM International: West Conshohocken, PA (2016).
29. ASTM C31 Practice for making and curing concrete test specimens in the field. ASTM International: West Conshohocken, PA (2010).
30. ASTM C1231 Practice for use of unbonded caps in determination of compressive strength of hardened concrete cylinders. ASTM International: West Conshohocken, PA (2015).
31. ASTM D2240 Test method for rubber property - Durometer hardness. ASTM International: West Conshohocken, PA (2017).
32. ASTM D412 Standard test methods for vulcanized rubber and thermoplastic elastomers. ASTM International: West Conshohocken, PA (2012).
33. ASTM D624 Standard test method for tear strength of conventional vulcanized rubber and thermoplastic elastomers. ASTM International: West Conshohocken, PA (2012).
34. BS 7976-2 Method of operation and calibration of the pendulum tester. British Standards Institution (2002).
35. J. D. Clarke *et al.*, Understanding the friction measured by standardised test methodologies used to assess shoe-surface slip risk, *J. Test. Eval.* **43** (2015) 723, <https://doi.org/10.1520/JTE20120334>.
36. ASTM E303 Standard test method for measuring surface frictional properties using the British pendulum tester. ASTM International: West Conshohocken, PA (2013).
37. S. K. Peddini *et al.*, Nanocomposites from styrene-butadiene rubber (SBR) and multiwall carbon nanotubes (MWCNT) part 2: mechanical properties, *Polymer* **56** (2015) 443, <https://doi.org/10.1016/j.polymer.2014.11.006>.
38. L. Aljerf, Effect of thermal-cured hydraulic cement admixtures on the mechanical properties of concrete, *Interceram - Int Ceram Rev* **64** (2015) 346, <https://doi.org/10.1007/BF03401142>.
39. I. Hutchings, P. Shipway, Tribology: Friction and wear of engineering materials, 2nd Ed. (Butterworth-Heinemann, 2017).